PHYSICAL REVIEW A VOLUME 34, NUMBER 5 NOVEMBER 1986

Strong velocity dependence of the atomic alignment effect in Na(3p)+Na(3p) associative ionization

M-X. Wang, J. Keller, J. Boulmer,* and J. Weiner
Department of Chemistry, University of Maryland, College Park, Maryland 20742
(Received 11 August 1986)

We have directly measured the effect of p-orbital spatial alignment on the associative-ionization (AI) cross section in $Na(3p)+Na(3p)$ collisions as a function of collision velocity in crossed atomic beams. Our measurements show that anisotropy in the cross section grows rapidly with velocity and that AI increasingly favors p-orbital alignment of both partners parallel to the laboratory collision axis over all other possible relative laboratory orientations.

Sensitivity to polarization alignment and orientation of excited-state reactants is proving to be a fruitful probe of the detailed dynamics in inelastic collision processes.[1-3] An experimentally tractable example is the associative-ionization (AI) process,

$$Na(3p)+Na(3p)\rightarrow Na_2^+ + e \ . \qquad (1)$$

Several recent experiments[4-7] have demonstrated that the thermally averaged cross section of process (1) has a small but significant dependence on the spatial alignment of the excited $Na(3p)$ orbitals. Kircz, Morgenstern, and Nienhuis[4] measured the AI rate in a single atomic beam experiment as a function of linear polarization angle. They found that the ionization rate exhibits a maximum when the excitation-laser polarization vector is aligned parallel to the atomic beam axis and a minimum when the alignment is perpendicular. Their results were later confirmed by several other[5-7] independent investigations.

In the present study, we have unfolded the thermally averaged alignment effect by directly measuring the velocity dependence over a range of collision energies from 0.018 to 0.274 eV. As described in an earlier report,[8] we achieve highly resolved velocity selection through laser excitation of narrow velocity groups in the Doppler profile of two crossed atomic beams. The experimental setup for the present measurement has been modified to achieve a wider accessible velocity range. For convenience, we describe here the general outline of the apparatus. Two atomic sources are oriented at 90° in the horizontal plane. Linearly polarized laser beams excite Na atoms to the $Na(3p\,^2P_{3/2})$ hyperfine manifold of states. In Fig. 1, we have depicted the excitation schemes used in achieving different combinations of $3p$-orbital alignments. Ultraviolet radiation from a high-pressure mercury lamp is at times collimated and focused into the collision region. The uv source, filtered to pass light between 2600 and 4000 Å, selectively photoionizes only excited $Na(3p)$ atoms; we use the amplitude of the photoionization signal to monitor the densities of the excited atomic beams. Ions are extracted by an electric field and detected by a particle multiplier. The dye-laser frequency (bandwidth 2 MHz) is repetitively swept over the Doppler profile of the atomic beams. Dimer-ion profiles from AI and atomic-ion profiles from excited-state photoionization are then averaged separately and recorded with a digital oscilloscope (Lecroy 9400) and plotter.

The basic rate equation for AI is given by

$$d[Na_2^+]/dt = \sigma_{AI} v [Na(3p)]_1 [Na(3p)]_2 \ , \qquad (2)$$

where σ_{AI} is the AI cross section and v is the collision velocity. The subscripts 1, 2 on $[Na(3p)]$ label the densities in atomic beams 1 and 2. The photoionization rate equation for $Na(3p)$ is given by

$$d[Na^+]/dt = \sigma_{ph}\Phi_{ph}[Na(3p)] \ , \qquad (3)$$

where σ_{ph} is the photoionization cross section and Φ_{ph} the photon flux of the photoionizing (uv) source. From Eqs. (2) and (3) we have

$$\sigma_{AI} = \frac{d[Na_2^+]/dt}{d[Na^+]_1/dt \cdot d[Na^+]_2/dt} (\Phi_{ph}\sigma_{ph})^2 \frac{1}{v} \ . \qquad (4)$$

The collision velocity v is determined from the frequency of the excitation laser [through the Doppler relation $v=\lambda_0(\nu-\nu_0)$] and the geometries of the excitation schemes (Fig. 1). The absolute frequency of the laser is determined from an iodine calibration spectrum measured concurrently with the sodium spectra. By measuring the ratio of Na_2^+ signal to the product of Na^+ intensities from each atomic beam as a function of the excitation laser frequency, we obtain the AI cross section as a function of col-

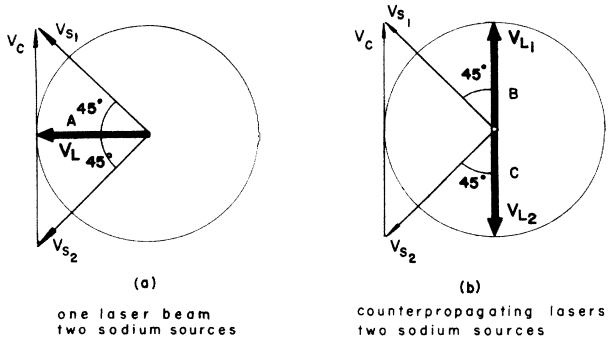

FIG. 1. Schematic diagram of laser-beam, atomic-beam laboratory setup. The labels V_{S_1} and V_{S_2} refer to velocity vectors from atomic beam sources 1 and 2, respectively. Labels V_{L_1} and V_{L_2} denote the laser-selected velocity component of each atomic beam. Labels A, B, C are the laser propagation paths used in these experiments, and V_C is the collision velocity.

lision velocity.

An experimental run proceeds as follows. The dye-laser frequency is scanned over the excitation profile of each atomic beam. With the uv source blocked, the ion signal arises entirely from associative ionization. With the uv source unblocked, the ion signal is the sum of AI and photoionization from Na($3p$). Associative ionization, however, produces a negligible contribution to the sum since the photoionization rate is greater than the AI rate by about two orders of magnitude. We check ion identities by time-of-flight mass analysis under all conditions of atomic beam irradiation. Systematic studies of light-intensity attenuation versus signal count rate confirmed linearity of the Na^+ signal with uv flux and quadratic dependence of the Na_2^+ signal with resonant laser flux.

The result of a typical ion profile measurement is shown in Fig. 2. We avoid overlapping contributions to the AI signal from $F=1$ and $F=2$ hyperfine levels of Na($3s\,^2S_{1/2}$) by restricting our measurements to frequencies red shifted from the rest frequency of the $F=2 \rightarrow F'=3$ transition. Laser propagation along paths B and C (Fig. 1), together with the red-shift restriction on the sweep range, permits excitation of each atomic beam separately. Thus the laser beam along path B excites Na beam 2, while the beam counter propagating along C excites Na beam 1. Selective excitation of each atomic beam provides a convenient means of measuring the separate atomic beam intensities, the product of which is required for determination of the AI cross section [Eq. (4)].

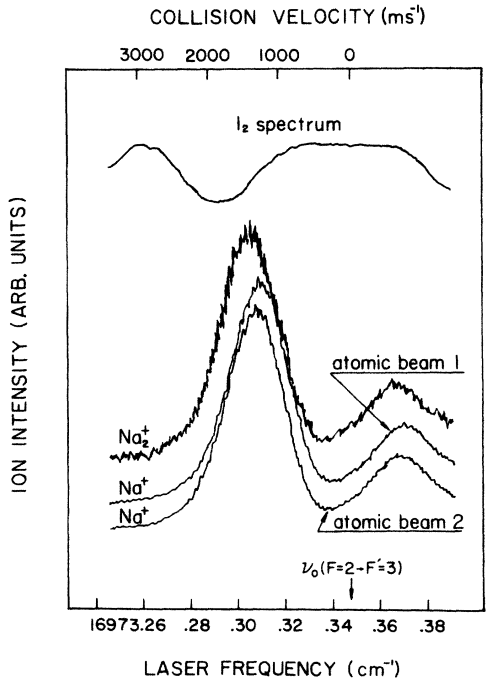

FIG. 2. Typical signal profiles showing the two atomic beam velocity distributions and the corresponding Na_2^+ velocity profile arising from AI (axial-axial approach). Curves have been vertically displaced for clarity. The I_2 spectrum is used for absolute frequency calibration. Small peaks on the right correspond to transition from Na($3s^2S_{1/2}, F=1$). Large peaks on the left arise from $F=2$ transitions.

We measure the AI signal in four different combinations of linear polarizations. The term "axial" refers to the laser polarization vector aligned coaxially with the relative velocity vector; the term "transverse" means laser polarization aligned perpendicular to the collision plane. The *relative* orientation of the two polarization vectors is indicated in parentheses.

(1) Axial-axial approach $\sigma_{\infty\infty}$: Horizontally polarized light propagates along A path, exciting both atomic beams.

(2) Transverse-transverse (parallel) approach σ_{88}: Vertically polarized light introduced along B (C) path excites atomic beam 2 (1).

(3) Transverse-transverse (perpendicular) approach $\sigma_{8\odot}$: Vertically and horizontally polarized light beams introduced along B and C paths, respectively.

(4) Axial-transverse approach $\sigma_{\infty 8}$: Vertically polarized laser light propagates along B path to excite atomic beam 2, and horizontally polarized light beam is introduced along A path to excite both beams. The signal thus obtained is a sum of $\sigma_{\infty 8}$ and $\sigma_{\infty\infty}$ from which $\sigma_{\infty 8}$ is determined by subtraction.

Calculation of the average collision velocity requires careful consideration of the details of the laser excitation process. Dipole selection rules permit linearly polarized light to excite transitions from the $3s\,^2S_{1/2}, F=2$ level to three hyperfine levels ($3p\,^2P_{2/3}, F'=3,2,1$). Hyperfine splitting between F' levels (shown in Fig. 3) means that each transition corresponds to a distinct velocity group in the Doppler profile of the atomic beam. Thus the observed AI cross section includes contributions from all three F' levels and the average collision velocity must be determined by weighting the three velocity groups according to their relative populations and to their positions on the Doppler velocity distribution. Excitation by linearly polar-

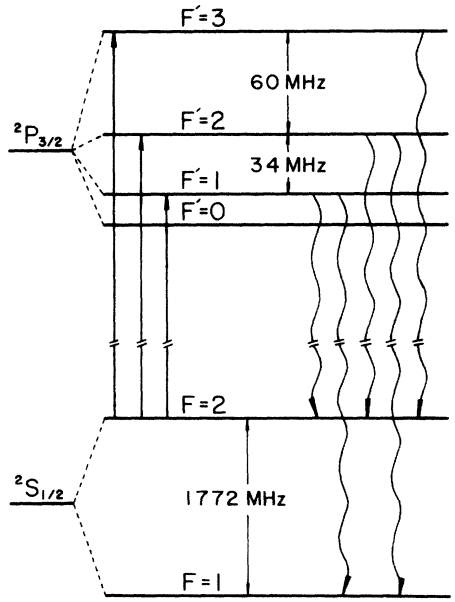

FIG. 3. Hyperfine energy levels for Na($3s^2S_{1/2}$) and Na($3p^2P_{3/2}$). Arrows indicate stimulated absorption and subsequent spontaneous deexcitation.

ized light results in optical pumping into $F=1$ of the ground state, and the rate of optical pumping is dependent on laser power. Therefore, it is important to characterize the time dependence of the excited-state populations and the effect of laser intensity on the rate of optical pumping into $Na(3s^2S_{1/2}, F=1)$. Figure 3 outlines the population flow among the various levels coupled by dipole transitions. We evaluate the time dependence of this population flow by solving the appropriate set of coupled differential equations, taking into account spontaneous emission and the power-broadened Lorentzian linewidth of each level. Figure 4 shows the results of this computer modeling from which we find the fractional population $P(i)$ $(i=3,2,1)$ of each velocity group during the time that Na atoms are in the collisional interacting region. In the numerical study we varied the laser power by a factor of 4 (6–24 mW) and found that the population of $F'=3$ increased with respect to the sum of populations in $F'=2,1$ by only about two percent. Then we cross checked the computer simulation by directly measuring the polarization anisotropy of the AI cross section as a function of laser intensity over the range 3–30 mW. We found an increase in the ratio $\sigma_{\infty\infty}/\sigma_{88}$ of a few percent, consistent with the numerical results. Having obtained the F' populations, we evaluate the peak positions in the speed distribution function of the atomic beam at temperature T (essentially Maxwell-Boltzmann) for each velocity group, $f_T(i)$ $(i=3,2,1)$. The average collision velocity is then calculated from

$$\langle v\rangle=\sum_i P(i)f_T(i)v_i \ . \tag{5}$$

In Fig. 5, we have plotted the AI cross section as a function of the average collision velocity for the various combinations of linear polarizations. From the result, we see that the cross sections for the four different combinations

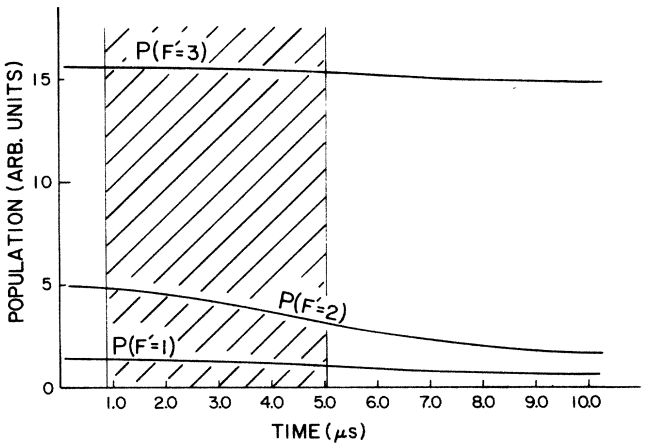

FIG. 4. Time dependence of F' level population as calculated by computer simulation. The shaded area indicates the time window during which the collision products of irradiated atoms are detected. The indicated window corresponds to the $F'=3$ velocity group; windows for $F'=2,1$ will be slightly smaller. The window width varies between 2 to 7 μs over the entire velocity profile.

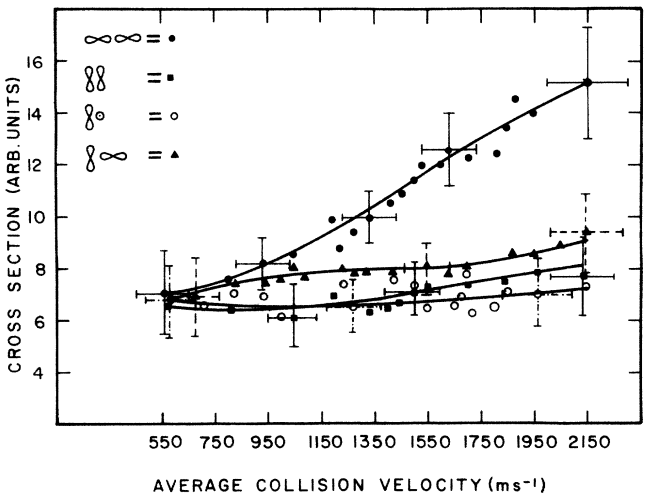

FIG. 5. AI cross sections as a function of average collision velocity for four different combinations of linear polarization. The average collision velocity is calculated from Eq. (5). Note the dramatic increase in cross section of axial-axial approach with increasing velocity.

of linear polarizations are close to each other at low collision velocities ($E=0.018$ eV), but $\sigma_{\infty\infty}$ dramatically increases at high energies while $\sigma_{\infty 8}$, σ_{88}, and $\sigma_{8\odot}$ remain relatively constant with $\sigma_{\infty 8}$ slightly larger than σ_{88} and $\sigma_{8\odot}$. At a collision energy of 0.274 eV ($v=2137$ m/s), $\sigma_{\infty\infty}$ is larger than the rest of the cross sections by about a factor of 2. Error bars on the abscissa are calculated from laser linewidth and long-term frequency drift as well as the finite collimation of the atomic beams. Uncertainties in AI cross section are determined from particle-counting statistics in Na^+ and Na_2^+. Error in the velocity measurement propagates through to the cross section determination via Eq. (4).

In order to check the consistency of the present results with the thermally averaged polarization effect measured previously,[7] we averaged $\sigma_{\infty\infty}$ and σ_{88} over the speed distribution appropriate to two atomic beams crossed at 180° and oven temperature of 635 K (conditions of Ref. 7). We calculate the thermally averaged ratio of $\sigma_{\infty\infty}/\sigma_{88}$ to be 1.7 ± 0.3 which is in good agreement with the measured ratio of 1.8 reported in Ref. 7.

The strong velocity dependence of the alignment in AI is a notable example of evidence for nonadiabatic coupling effects between quasimolecular states of the approaching collision partners. Although the specific nature of these nonadiabatic processes is as yet unknown, we note that the polarized excitation prepares the electron orbital angular momentum alignment, and that the spin-orbit coupling time (Larmor-precession period) is comparable to the time of collision. We speculate that as the relative velocity increases, spin-orbit recoupling has less time to scramble the initially prepared electron orbital alignment, resulting in enhanced anisotropy in the AI cross section. A detailed analysis of this velocity-dependent alignment effect remains to be worked out and will be the subject of future studies.

We thank Mr. M. H. Ghatee for assistance in the experiment and computer simulations. Computer time for this project was supported through the facilities of the Computer Science Center of the University of Maryland. Support from the National Science Foundation under Grant No. PHY-8503501 is gratefully acknowledged.

---

*Permanent address: Institut d'Electronique Fondamentale, Bâtiment 220, Faculté d'Orsay, F-91405 Orsay, France.

[1]C. T. Rettner and R. N. Zare, J. Chem. Phys. **77**, 2416 (1982).

[2]M. O. Hale, I. V. Hertel, and S. R. Leone, Phys. Rev. Lett. **53**, 2296 (1984).

[3]A. Bahring, I. V. Hertel, E. Meyer, and H. Schmidt, Phys. Rev. Lett. **53**, 1433 (1984).

[4]J. C. Kircz, R. Morgenstern, and G. Nienhuis, Phys. Rev. Lett. **48**, 610 (1982).

[5]E. W. Rothe, R. Theyunni, G. P. Reck, and C. C. Tung, Phys. Rev. A **33**, 1426 (1986).

[6]M-X. Wang, M. S. de Vries, and J. Weiner, Phys. Rev. A **33**, 765 (1986).

[7]H. A. J. Meijer, H. P. v. d. Meulen, R. Morgenstern, I. V. Hertel, E. Meyer, H. Schmidt, and R. Witte, Phys. Rev. A **33**, 1421 (1986).

[8]M-X. Wang, M. S. de Vries, J. Keller, and J. Weiner, Phys. Rev. A **32**, 681 (1985).